

Diagnosing quantum crosstalk in superconducting quantum chips by using out-of-time-order correlators

Yujia Zhang(张宇佳), Yu Zhang(张钰), Shaoxiong Li(李邵雄), Wen Zheng(郑文), and Yang Yu(于扬)

Citation: Chin. Phys. B, 2024, 33 (**11**): 110306. DOI: 10.1088/1674-1056/ad73b3
Journal homepage: http://cpb.iphy.ac.cn; http://iopscience.iop.org/cpb

What follows is a list of articles you may be interested in

Remote entangling gate between a quantum dot spin and a transmon qubit mediated by microwave photons

Xing-Yu Zhu(朱行宇), Le-Tian Zhu(朱乐天), Tao Tu(涂涛), and Chuan-Feng Li(李传锋)
Chin. Phys. B, 2024, 33 (**2**): 020315. DOI: 10.1088/1674-1056/ad1747

Fast and perfect state transfer in superconducting circuit with tunable coupler

Chi Zhang(张驰), Tian-Le Wang(王天乐), Ze-An Zhao(赵泽安), Xiao-Yan Yang(杨小燕), Liang-Liang Guo(郭亮亮), Zhi-Long Jia(贾志龙), Peng Duan(段鹏), and Guo-Ping Guo(郭国平)
Chin. Phys. B, 2023, 32 (**11**): 110305. DOI: 10.1088/1674-1056/acf496

Realization of high-fidelity and robust geometric gates with time-optimal control technique in superconducting quantum circuit

Zhimin Wang(王治旻), Zhuang Ma(马壮), Xiangmin Yu(喻祥敏), Wen Zheng(郑文), Kun Zhou(周坤), Yujia Zhang(张宇佳), Yu Zhang(张钰), Dong Lan(兰栋), Jie Zhao(赵杰), Xinsheng Tan(谭新生), Shaoxiong Li(李邵雄), and Yang Yu(于扬)
Chin. Phys. B, 2023, 32 (**10**): 100304. DOI: 10.1088/1674-1056/ace15b

Entanglement properties of superconducting qubits coupled to a semi-infinite transmission line

Yang-Qing Guo(郭羊青), Ping-Xing Chen(陈平形), and Jian Li(李剑)
Chin. Phys. B, 2023, 32 (**6**): 060302. DOI: 10.1088/1674-1056/acc0fa

Quantum computation and simulation with superconducting qubits

Kaiyong He(何楷泳), Xiao Geng(耿霄), Rutian Huang(黄汝田), Jianshe Liu(刘建设), and Wei Chen(陈炜)
Chin. Phys. B, 2021, 30 (**8**): 080304. DOI: 10.1088/1674-1056/ac16cf

---

Diagnosing quantum crosstalk in superconducting quantum chips by using out-of-time-order correlators

Yujia Zhang(张宇佳)[1,2,3], Yu Zhang(张钰)[1,2,3,†], Shaoxiong Li(李邵雄)[1,2,3,4], Wen Zheng(郑文)[1,2,3], and Yang Yu(于扬)[1,2,3,4]

[1] *National Laboratory of Solid State Microstructures, School of Physics, Nanjing University, Nanjing* 210093, *China*
[2] *Shishan Laboratory, Suzhou Campus of Nanjing University, Suzhou* 215163, *China*
[3] *Synergetic Innovation Center of Quantum Information and Quantum Physics, University of Science and Technology of China, Hefei* 230026, *China*
[4] *Hefei National Laboratory, Hefei* 230088, *China*

(Received 11 June 2024; revised manuscript received 19 August 2024; accepted manuscript online 27 August 2024)

Performance of a scalable quantum processor critically relies on minimizing crosstalk and unwanted interactions within the system, as it is vital for parallel controlled operations on qubits. We present a protocol not only to provide information about residual coupling but also to effectively discriminate it from the influence of classical crosstalk. Our approach utilizes out-of-time-order correlators (OTOCs) as a signal of quantum crosstalk, making it applicable to various coupling forms and scalable architectures. To demonstrate the effectiveness of our protocol, we provide a theoretical analysis and simulate its implementation in coupled superconducting qubits.

Keywords: superconducting qubit, crosstalk, out-of-time-order correlator (OTOC)

PACS: 03.67.Lx, 85.25.Cp, 02.70.–c **DOI:** 10.1088/1674-1056/ad73b3

1. Introduction

High-precision quantum operation is vital for performance of quantum information processors (QIP) in the noisy intermediate-scale quantum era. Accurately calibrating the parameters of a QIP is essential to attain such high precision. With increasing number of qubits and complexity of circuitry, it is a big challenge to calibrate those parameters involving multiple qubits. Among others, crosstalk not only distorts the state of individual qubits but also leads to decreased performance in parallel gate operations. For instance, isolated single-qubit gates in superconductor qubits exhibit fidelities exceeding 99.9% and even 99.99%,[1–3] while two-qubit gates also achieve 99.9% fidelity.[4,5] However, when performing gate operations in parallel, it has been commonly observed that the gate performance deteriorates.[6–8]

In the superconducting QIPs, the crosstalk can be categorized into two distinct types based on their origins. The first type is classical crosstalk, the effect on qubit i by a classical control signal applied on another qubit j, which can be generally expressed as a single qubit operator $s_{ij}\hat{\sigma}_i$, where s_{ij} is the crosstalk matrix and $\hat{\sigma}$ represents the Pauli operator. For superconducting QIPs, the classical control signal can be a flux bias or a microwave field. The second type is quantum crosstalk, arising from parasitic interaction between qubits,[7] which can be represented as $\hat{\sigma}_i\hat{\sigma}_j$ for two-qubit interaction. Quantum crosstalk, in particular, introduces unwanted correlations that can be highly detrimental to error correction.[9–12] Two types of crosstalk are usually minimized by exploiting difference strategies. The classical crosstalk can effectively be identified and mitigated by compensating with opposing control signals, as demonstrated in the studies of Refs. [13–16]. On the other hand, the quantum crosstalk can be minimized by carefully designing the layout of the qubits and incorporating additional elements such as couplers.[17,18] There also frequently appears that two types of crosstalk are interwinded together when operating entangling gate. It is therefore desirable to find a way that can be used to distinguish these two crosstalks clearly and is also sensitive for crosstalks at the same time.

In this work, we propose to use out-of-time-order correlators (OTOCs) as a signal to single out quantum crosstalk, which is also a sensitive tool for diagnosing crosstalk. The OTOC is overlapping between two quantum states. One quantum state is obtained by applying an operator $\hat{V}$ on the system, evolving for time t, applying an opeartor $\hat{W}$, and finally evolving for time $-t$. The other state is obtained by evolving for time t, applying $\hat{W}$, evolving for time $-t$, and finally applying $\hat{V}$. The concept of OTOC was initially introduced in the field of superconductivity literature.[19] In recent years, it has been found that the decay of OTOC can be used as a metric characterizing the spreading of quantum information in various domains. Examples include the study of the black hole information problem,[20,21] many-body localization (MBL) systems,[22–32] and the quantum behavior of chaotic systems.[33,34] Compared to previous proposals, such as process tomography, simultaneous gate set

†Corresponding author. E-mail: smutnauq@nju.edu.cn

© 2024 Chinese Physical Society and IOP Publishing Ltd

tomography,[35] many-qubit randomized benchmarking,[36] simultaneous randomized benchmarking,[6] and Hamiltonian tomography,[37,38] etc., our approach offers three notable advantages. First, our approach eliminates the requirement for entanglement gates, making it more convenient for experimentation. Second, the decay rate of the OTOC can reflect the strength of residual coupling. Third, the OTOC allows us to eliminate the interference caused by classical crosstalk and focus exclusively on quantum crosstalk.

2. Model and proposal

The OTOC is derived from the squared commutator which can quantify the impact spreading of a local operator in a quantum lattice:

$$C_{W,V}(t) = \langle [\hat{W}(t), \hat{V}]^{\dagger} [\hat{W}(t), \hat{V}] \rangle, \tag{1}$$

where $\hat{V}$ denotes a local operator applied at one lattice site, which can cause perturbation spreading throughout the lattice. Similarly, $\hat{W}$ represents another local operator applied at a different site, evolving for time t, and then evolving back for time $-t$, expressed as $\hat{W}(t) = \mathrm{e}^{\mathrm{i}\hat{H}t}\hat{W}\mathrm{e}^{-\mathrm{i}\hat{H}t}$. This evolution causes $\hat{W}(t)$ to propagate across multiple sites, and if $\hat{V}$ lies within its light cone, the commutator $C(t)$ will be nonzero. Both $\hat{V}$ and $\hat{W}$ are assumed to be Hermitian and unitary operators. The commutator $C(t)$ can be expressed as $C(t) = 2 - 2\mathrm{Re}[F(t)]$, where $F_{W,V}(t) = \langle \hat{W}(t)\hat{V}^{\dagger}\hat{W}(t)\hat{V} \rangle$ is known as the OTOC. The decay of the OTOC from 1 is the only factor that allows the correlator to increase.

For concreteness of discussions, we discuss our proposal on superconducting quantum circuits, a rapidly developing and extensively studied area. However, it is important to note that the principles of our proposal are applicable to any quantum information processor. Since the convenient architecture of a superconducting quantum chip is two-dimensional (2D), here we consider 2D qubit grids as shown in Fig. 1, where $\hat{V}$ and $\hat{W}$ are applied to two distinct grid points, respectively. If there is no effective coupling between these points, regardless of the placement and types of $\hat{V}$ and $\hat{W}$, the OTOC will remain at 1. However, in the presence of effective coupling between qubits, $\hat{V}$ will become nonlocal and propagate across the entire system. As the time-evolved operator $\hat{W}(t)$ overlaps with $\hat{V}$ and generates noncommuting terms, the OTOC begins to decay. The closer $\hat{W}(t)$ is applied, the earlier the decay of the OTOC occurs. Furthermore, the strength of the effective coupling g determines the rate of decay in the OTOC over time. By applying $\hat{W}(t)$ and $\hat{V}$ at two different positions of interest, we can utilize the decay rate of the OTOC to characterize the presence of quantum crosstalk between qubits. Since the classical crosstalk manifests itself as a single Pauli operator at another grid point, rather than a direct product of two Pauli operators, the classical crosstalk does not introduce noncommutative terms and therefore does not lead to the decay of OTOC. Based on its distinct properties on quantum and classical crosstalk, OTOCs could be instrumental for calibrating crosstalk in quantum chips.

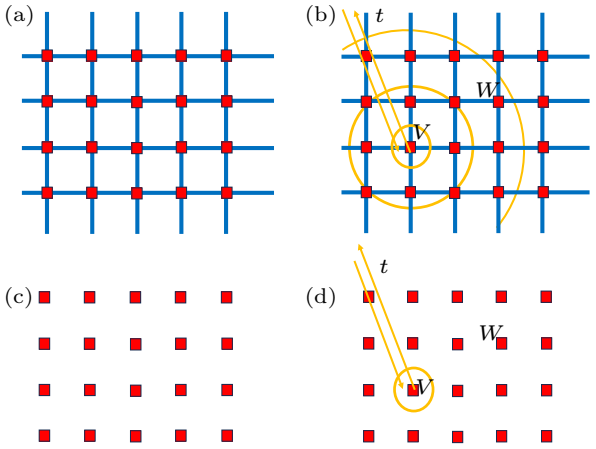


Fig. 1. Probing quantum crosstalk via OTOCs in 2D qubit grids. (a) A 2D qubit grid with coupling. (b) The initial perturbation $\hat{V}$ scrambled into non-local qubit lattice. If an additionally perturbed $\hat{W}$ applied before rewinding time and falls within the light cone of $\hat{V}$, the scrambling will be captured by the squared commutator C. (c) A 2D qubit grid without coupling. (d) The initial perturbation $\hat{V}$ remains localized, and the squared commutator C retains a value of 1.

To verify our proposal, we numerically investigate OTOC's distinct behaviors of quantum and classic crosstalk. We focus our analysis and calculations on the smallest building block of the 2D qubit grids:[39,40] four fixed-frequency qubits arranged in a rectangular configuration with controllable coupling between them, as depicted in Fig. 2(a). The Hamiltonian of the system can be expressed as

$$\hat{H} = \sum_{l} [\omega_l \hat{a}_l^{\dagger}\hat{a}_l + \frac{\eta}{2}\hat{a}_l^{\dagger}\hat{a}_l^{\dagger}\hat{a}_l\hat{a}_l + g_l(\hat{a}_l^{\dagger}\hat{a}_{l+1} + \hat{a}_l\hat{a}_{l+1}^{\dagger})], \tag{2}$$

where the subscript $l \in \{0,1,2,3\}$ represents l-th oscillator {Q0, Q1, Q2,Q3} with anharmonicity η_l and frequency ω_l; $\hat{a}_l$ ($\hat{a}_l^{\dagger}$) is the associated annihilation (creation) operator, and g_l denotes the nearest-neighbor (NN) coupling strength. The qubits are resonant at $\omega/2\pi = 5.0$ GHz. Both couplers and qubits are three-level truncated. The initial state is $|1000\rangle$. Note that the typical arrangement of the qubit frequencies in a chip is staggered. The choice of the resonant qubits here is intended to conveniently demonstrate the impact of the crosstalk. Moreover, our numerical simulation indicates that it does not bring in any qualitatively differences with the staggered frequencies.

For convenience, the operator $\hat{V}$ is always applied at Q0 in our numerical simulations. To show the sensitivity of OTOC on g, we apply probing operator $\hat{W} = \hat{\sigma}_z$ on the next near qubit Q2 with $\hat{V} = \hat{\sigma}_z$. The dependence of OTOC with evolution time for different g values is shown in Fig. 2(b). Since the crosstalk is our concern, g takes the same and relatively small value for all neighboring qubits here for simplicity. It is clear that the impact of g on the decay rate of OTOC is evident in

Fig. 2(b) at least for short time scale ($t < 0.5$ μs). Due to the fact that the Hamiltonian we adopted is integrable,[28,41] The OTOC exhibits certain oscillation for $g/2\pi = 0.2$ MHz. Note that OTOC has been employed to characterize operator spreading and information scrambling, a faster decay of OTOC with larger g indicates faster information propagating. We also show the dependence of OTOC on coupling distance in Fig. 2(c). For comparison, $\hat{W}$ is applied at Q1 and Q2, respectively. When $\hat{W}$ is applied at Q1, regardless of its type, the decay of OTOC occurs earlier than that with $\hat{W}$ at Q2, which can be attributed to the fact that the spreading of $\hat{W}$ to Q0 requires more time when $\hat{W}$ is further away from $\hat{V}$. In Fig. 2(c), it can be found that the overall amplitude of F_{ZZ} is smaller than that of F_{XX}, which is due to the fact that F_{ZZ} involves more high-order oscillation-in-time terms for the studied system.

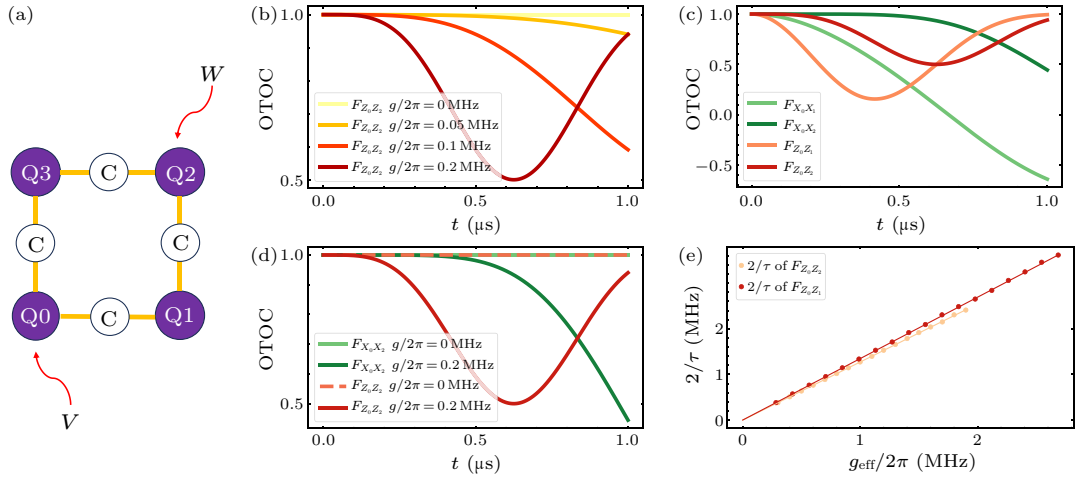


Fig. 2. Probing quantum crosstalk via OTOCs in a 2×2 four-qubit square. (a) Sketch of a generic a 2×2 four-qubit square, where the connecting lines represent tunable couplings. Localization operators $\hat{W}$ and $\hat{V}$ are applied to two specific qubits, respectively. (b) OTOC versus evolution time t for different $g/2\pi = 0, 0.05, 0.1, 0.2$ MHz, with $\hat{V}$, $\hat{W} = \hat{\sigma}_z$ applied at Q0 and Q2, respectively. (c) OTOC versus t for a fixed $g/2\pi = 0.2$ MHz with $\hat{W}$ at Q1 or Q2. (d) OTOC versus t with $(\hat{V}, \hat{W})$=$(\hat{\sigma}_x, \hat{\sigma}_x)$ and $(\hat{\sigma}_z, \hat{\sigma}_z)$, $\hat{W}$ at Q2, $g/2\pi = 0.2$ MHz and 0 MHz, respectively. (e) The inverse of the time at which F_{ZZ} reaches the first obvious local minimum τ versus the effective coupling $g_{\rm eff}$. Dots are the simulation results and solid lines are the linear fits to the data.

To demonstrate the distinct behaviors of the OTOCs for quantum and classic crosstalk, Fig. 2(d) shows the calculated dependence of OTOCs with quantum and classic crosstalk. Here, $\hat{W}$ is applied at Q2, $\hat{V}$ and $\hat{W}$ are chosen as $\hat{\sigma}_x, \hat{\sigma}_x$ or $\hat{\sigma}_z, \hat{\sigma}_z$. In the absence of coupling ($g = 0$), a perturbation applied to a single qubit does not disturb the commutator between qubits. Thus, in the case of classical crosstalk alone, it can not influence the OTOC. However, if $g \neq 0$, the OTOC will begin to decay over time as the operator $\hat{W}$ eventually falls within the light cone of the operator $\hat{V}$.

The strength of the residual coupling g can be inferred from OTOCs. For the resonant qubits, the effective coupling $g_{\rm eff}$ in 2D qubit lattice can be defined according to the propagation velocity of quantum walk.[42,43] The effective coupling is given by $g_{\rm eff} = 2\sqrt{2}g(1 - \frac{16g^2}{9\eta^2})/d$, where d is the distance between two coupled sites. For examples, $d = 1$ for the coupling between Q_0 and Q_1, $d = \sqrt{2}$ for the coupling between Q_0 and Q_2. Our numerical simulations find that the inverse of the time at which F_{ZZ} reaches the first obvious local minimum τ is proportional to $g_{\rm eff}$. For both $F_{Z_0Z_1}$ and $F_{Z_0Z_2}$, $2/\tau$ is linearly related to $g_{\rm eff}$, as illustrated in Fig. 2(e).

It is obvious that the term in the Hamiltonian, which can contribute to OTOCs, does not commute with $\hat{W}$ and $\hat{V}$. We have the flexibility to choose different $\hat{W}$ and $\hat{V}$ in order to resolve special residual coupling. For example, $(\hat{V}, \hat{W})$=$(\hat{\sigma}_z, \hat{\sigma}_z)$ can be used to resolve transverse coupling (hereinafter referred to as XX coupling).

To show this kind of distinguishing, we consider a specific qubit-coupler-qubit chain system with three qubits in total and the tunable coupler in between, where the qubit is transmon,[44] the coupler is tunable with frequency below the qubit frequency.[18,45] The qubits are also resonant at $\omega/2\pi = 5.0$ GHz and labeled as 0, 1, and 2. The initial state is $|100\rangle$. The couplers are operated at the same frequency. A moving average process is used to eliminate the obvious feature related to the detuning between the qubit and the coupler when calculating the OTOC.

The typical tuning of the coupler is shown in Fig. 3(a). The coupler tuned at certain frequencies ($\omega_c/2\pi$) can turn off XX interaction (g) or ZZ interaction ($\xi = E_{11} - E_{01} - E_{10} + E_{00}$), while two types of off-points are not exactly coincidence. The decay rate of the OTOC with $(\hat{V}, \hat{W})$=$(\hat{\sigma}_z, \hat{\sigma}_z)$ qualitatively agrees with the corresponding XX-coupling strength. When the coupler is tuned at the XX off-point, the OTOC experiences little decay, as illustrated in Fig. 3(b). The results also show that, following a decay, OTOCs revive almost back to the initial value $+1$, since the system's Hamiltonian is integrable.[28,41] The OTOC reflects the effective XX-coupling between qubits, the trend of it changing with frequency is also basically consistent with the tuning of the coupler, as depicted

in Fig. 3(c).

In superconducting circuits the transverse coupling contains both $\hat{\sigma}_x\hat{\sigma}_x$ and $\hat{\sigma}_y\hat{\sigma}_y$. It is impossible to detect ZZ coupling by simply using F_{XX} or F_{YY} only. However, by carefully comparing F_{XX} and F_{ZZ}, one can tell whether ξ approximates zero. We numerically demonstrate the behaviors of F_{XX} and F_{ZZ} with ZZ coupling and without ZZ coupling. In our numerical simulation, the couplers are tuned at $\omega_c/2\pi = 4.1$ GHz, 4.175 GHz, 4.45 GHz, corresponding to the couplings with ZZ only, XX only, and both XX and ZZ, respectively. The behaviors of $F_{X_0X_1}$ and $F_{Z_0Z_1}$ at these points are illustrated in Figs. 3(d)–3(f). Fourier transforms are used to reveal the frequency features of the calculated OTOCs, as depicted in Figs. 3(g)–3(i). At the XX off-point, $F_{Z_0Z_1}$ exhibits little decay or oscillation with time, which indicates the absence of the XX coupling. $F_{X_0X_1}$ shows slight decay with time, which is due to the residue ZZ coupling. The frequency domain data confirms the features observed in the time domain. At the ZZ off-point, $F_{Z_0Z_1}$ displays a single-frequency oscillation for the XX coupling. $F_{X_0X_1}$ exhibits multiple frequency components. The appearing multiple frequency components may be due to incomplete suppression of the ZZ coupling. With the XX coupling of 33 MHz and the ZZ coupling of 2.9 MHz, $F_{Z_0Z_1}$ also shows a clear oscillation. $F_{X_0X_1}$ contains not only its fractional or same frequency but also obvious other frequency components, such as its second peak, an implication of the ZZ coupling.

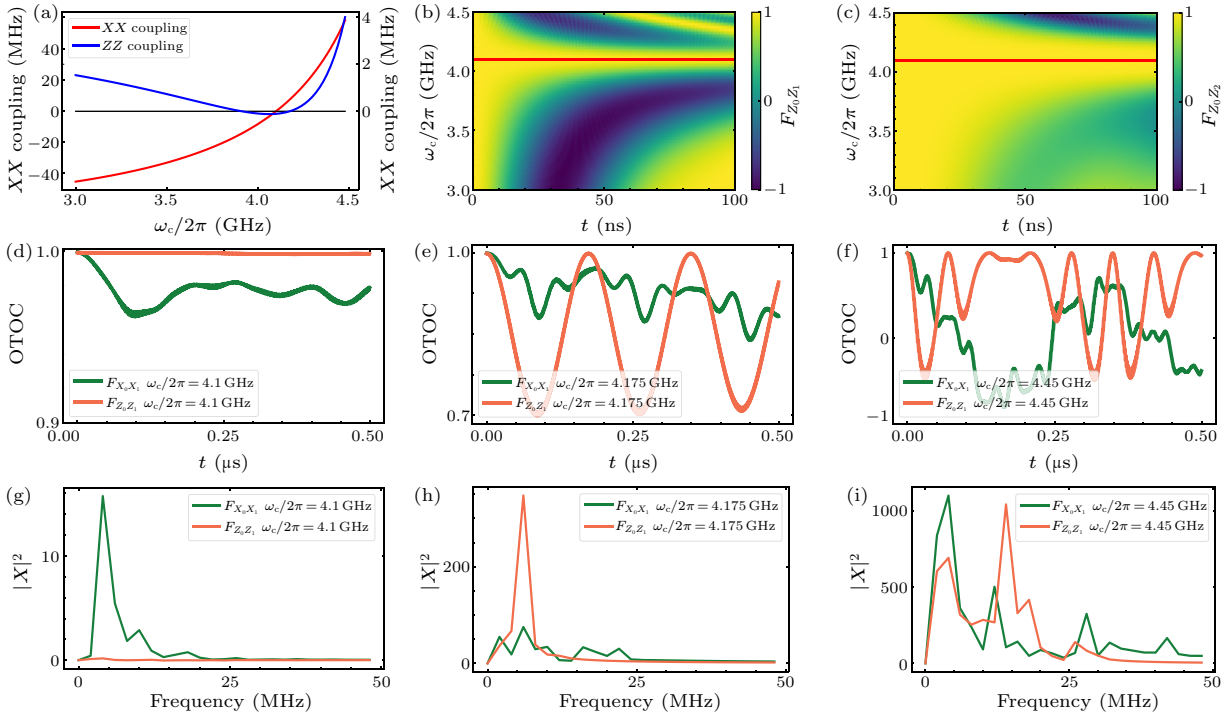


Fig. 3. Discriminating only XX-coupling using OTOCs. (a) ZZ-coupling and XX-coupling tuning with a tunable coupler, where the off-point of XX is at coupler frequency $\omega_c/2\pi = 4.100$ GHz. The off-points of ZZ are at $\omega_c/2\pi = 3.913$ GHz and $\omega_c/2\pi = 4.175$ GHz. (b) $F_{Z_0Z_1}$ versus ω_c and t. (c) $F_{Z_0Z_2}$ versus ω_c and t. The red horizontal line indicates XX off-point. $F_{Z_0Z_1}$ and $F_{X_0X_1}$ versus t with (d) $\omega_c/2\pi = 4.10$ GHz, (e) $\omega_c/2\pi = 4.175$ GHz and (f) $\omega_c/2\pi = 4.45$ GHz. (g)–(i) The corresponding frequency spectra obtained from Fourier transform.

The big challenge for measurement of OTOC with weak residual coupling is evolving back $[U(-t)]$ with high fidelity. To find the accurate $U(-t)$, we can try OTOC with $\hat{W} = \mathrm{I}$. When $U(t) = U(-t)$ accurately, the OTOC only decays due to decoherence, does not oscillate. This method may also be utilized to accurately find off-coupling points of couplers. When $U(-t)$ is deviated, there will be a discrepancy between the slowest decay of OTOC and $g = 0$.

Though realizing time-reversal operations remains an experimental challenge, various experiment implementations across different systems have been successfully realized by changing the sign of detuning between qubits and applying specific gates,[30] changing the sign of coupling,[27,28] decomposing e^{iHt} into either single-spin operation or coupled two-spin operation.[25] Furthermore, alternative schemes that do not necessitate actual time-reversal have been proposed.[46] The impact of decoherence can be eliminated through a contrast experiment without $\hat{W}$.[47]

3. Conclusion

In summary, we have proposed an experimentally feasible approach to characterize residual coupling in quantum computers of any scale by using OTOCs. The proposed method could be used to effectively mitigate the disturbances caused by classical crosstalk, decoherence, and diagnose weak residual coupling. We have conducted our analysis specifically

within the superconducting transmon system.

Acknowledgments

Project supported by the National Natural Science Foundation of China (Grant Nos. 12074179 and U21A20436), the Innovation Program for Quantum Science and Technology (Grant No. 2021ZD0301702), the Natural Science Foundation of Jiangsu Province, China (Grant Nos. BE2021015-1 and BK20232002), and the Natural Science Foundation of Shandong Province (Grant No. ZR2023LZH002).

References

[1] Debroy D M, Li M, Huang S and Brown K R 2020 *Quantum Sci. Technol.* **5** 034002
[2] Chen Z, Kelly J, Quintana C, Barends R, Campbell B, Chen Y, Chiaro B, Dunsworth A, Fowler A G, Lucero E, Jeffrey E, Megrant A, Mutus J, Neeley M, Neill C, O'Malley P J J, Roushan P, Sank D, Vainsencher A, Wenner J, White T C, Korotkov A N and Martinis J M 2016 *Phys. Rev. Lett.* **116** 020501
[3] Somoroff A, Ficheux Q, Mencia R A, Xiong H, Kuzmin R and Manucharyan V E 2023 *Phys. Rev. Lett.* **130** 267001
[4] Ding L, Hays M, Sung Y, Kannan B, An J, Di Paolo A, Karamlou A H, Hazard T M, Azar K, Kim D K, Niedzielski B M, Melville A, Schwartz M E, Yoder J L, Orlando T P, Gustavsson S, Grover J A, Serniak K and Oliver W D 2023 *Phys. Rev. X* **13** 031035
[5] Negîrneac V, Ali H, Muthusubramanian N, Battistel F, Sagastizabal R, Moreira M S, Marques J F, Vlothuizen W J, Beekman M, Zachariadis C, Haider N, Bruno A and DiCarlo L 2021 *Phys. Rev. Lett.* **126** 220502
[6] Gambetta J M, Córcoles A D, Merkel S T, Johnson B R, Smolin J A, Chow J M, Ryan C A, Rigetti C, Poletto S, Ohki T A, Ketchen M B and Steffen M 2012 *Phys. Rev. Lett.* **109** 240504
[7] Zhao P, Linghu K, Li Z, Xu P, Wang R, Xue G, Jin Y and Yu H 2022 *PRX Quantum* **3** 020301
[8] Zajac D M, Stehlik J, Underwood D L, Phung T, Blair J, Carnevale S, Klaus D, Keefe G A, Carniol A, Kumph M, Steffen M and Dial O E 2021 arXiv:2108.11221 [quant-ph]
[9] Kitaev A Y 2003 *Ann. Phys.* **303** 2
[10] Huang C, Ni X, Zhang F, Newman M, Ding D, Gao X, Wang T, Zhao H H, Wu F, Zhang G, Deng C, Ku H S, Chen J and Shi Y 2020 arXiv:2002.08918 [quant-ph]
[11] Landahl A J, Anderson J T and Rice P R 2011 arXiv:1108.5738 [quant-ph]
[12] Devitt S J, Munro W J and Nemoto K 2013 *Rep. Prog. Phys.* **76** 076001
[13] Abrams D M, Didier N, Caldwell S A, Johnson B R and Ryan C A 2019 *Phys. Rev. Appl.* **12** 064022
[14] Dai X, Tennant D, Trappen R, Martinez A, Melanson D, Yurtalan M, Tang Y, Novikov S, Grover J, Disseler S, Basham J, Das R, Kim D, Melville A, Niedzielski B, Weber S, Yoder J, Lidar D and Lupascu A 2021 *PRX Quantum* **2** 040313
[15] Nuerbolati W, Han Z, Chu J, Zhou Y, Tan X, Yu Y, Liu S and Yan F 2022 *Appl. Phys. Lett.* **120** 174001
[16] Yan H, Zhao S, Xiang Z, Wang Z, Yang Z, Xu K, Tian Y, Yu H, Zheng D, Fan H, *et al.* 2023 *Chin. Phys. B* **32** 094203
[17] Yan F, Krantz P, Sung Y, Kjaergaard M, Campbell D L, Orlando T P, Gustavsson S and Oliver W D 2018 *Phys. Rev. Appl.* **10** 054062
[18] Sete E A, Chen A Q, Manenti R, Kulshreshtha S and Poletto S 2021 *Phys. Rev. Appl.* **15** 064063
[19] Larkin A I and Ovchinnikov Y N 1969 *Sov. Phys. JETP* **28** 1200
[20] Shenker S H and Stanford D 2014 *J. High Energy Phys.* **2014** 67
[21] Jahnke V, Kim K Y and Yoon J 2019 *J. High Energy Phys.* **2019** 37
[22] Huang Y, Zhang Y L and Chen X 2017 *Ann. Phys.* **529** 1600318
[23] Fan R, Zhang P, Shen H and Zhai H 2017 *Sci. Bull.* **62** 707
[24] Dağ C B and Duan L M 2019 *Phys. Rev. A* **99** 052322
[25] Li J, Fan R, Wang H, Ye B, Zeng B, Zhai H, Peng X and Du J 2017 *Phys. Rev. X* **7** 031011
[26] Wei K X, Ramanathan C and Cappellaro P 2018 *Phys. Rev. Lett.* **120** 070501
[27] Gärttner M, Bohnet J G, Safavi-Naini A, Wall M L, Bollinger J J and Rey A M 2017 *Nat. Phys.* **13** 781
[28] Zhao S K, Ge Z Y, Xiang Z, Xue G M, Yan H S, Wang Z T, Wang Z, Xu H K, Su F F, Yang Z H, Zhang H, Zhang Y R, Guo X Y, Xu K, Tian Y, Yu H F, Zheng D N, Fan H and Zhao S P 2022 *Phys. Rev. Lett.* **129** 160602
[29] Zhu Q, Sun Z H, Gong M, *et al.* 2022 *Phys. Rev. Lett.* **128** 160502
[30] Braumüller J, Karamlou A H, Yanay Y, Kannan B, Kim D, Kjaergaard M, Melville A, Niedzielski B M, Sung Y, Vepsäläinen A, Winik R, Yoder J L, Orlando T P, Gustavsson S, Tahan C and Oliver W D 2022 *Nat. Phys.* **18** 172
[31] Berke C, Varvelis E, Trebst S, Altland A and DiVincenzo D P 2022 *Nat. Commun.* **13** 2495
[32] Mi X, Roushan P, Quintana C, Mandra S, Marshall J, Neill C, Arute F, Arya K, Atalaya J, Babbush R, *et al.* 2021 *Science* **374** 1479
[33] Swingle B 2018 *Nat. Phys.* **14** 988
[34] Kukuljan I, Grozdanov S C V and Prosen T C V 2017 *Phys. Rev. B* **96** 060301
[35] Rudinger K, Hogle C W, Naik R K, Hashim A, Lobser D, Santiago D I, Grace M D, Nielsen E, Proctor T, Seritan S, Clark S M, Blume-Kohout R, Siddiqi I and Young K C 2021 *PRX Quantum* **2** 040338
[36] McKay D C, Sheldon S, Smolin J A, Chow J M and Gambetta J M 2019 *Phys. Rev. Lett.* **122** 200502
[37] Patterson A, Rahamim J, Tsunoda T, Spring P, Jebari S, Ratter K, Mergenthaler M, Tancredi G, Vlastakis B, Esposito M and Leek P 2019 *Phys. Rev. Appl.* **12** 064013
[38] Wang S T, Deng D L and Duan L M 2015 *New J. Phys.* **17** 093017
[39] Johansson J, Nation P and Nori F 2012 *Comput. Phys. Commun.* **183** 1760
[40] Johansson J, Nation P and Nori F 2013 *Comput. Phys. Commun.* **184** 1234
[41] Lin C J and Motrunich O I 2018 *Phys. Rev. B* **97** 144304
[42] Cheneau M, Barmettler P, Poletti D, Endres M, Schauß P, Fukuhara T, Gross C, Bloch I, Kollath C and Kuhr S 2012 *Nature* **481** 484
[43] Gong M, Wang S, Zha C, Chen M C, Huang H L, Wu Y, Zhu Q, Zhao Y, Li S, Guo S, *et al.* 2021 *Science* **372** 948
[44] Koch J, Yu T M, Gambetta J, Houck A A, Schuster D I, Majer J, Blais A, Devoret M H, Girvin S M and Schoelkopf R J 2007 *Phys. Rev. A* **76** 042319
[45] Stehlik J, Zajac D M, Underwood D L, Phung T, Blair J, Carnevale S, Klaus D, Keefe G A, Carniol A, Kumph M, Steffen M and Dial O E 2021 *Phys. Rev. Lett.* **127** 080505
[46] Vermersch B, Elben A, Sieberer L M, Yao N Y and Zoller P 2019 *Phys. Rev. X* **9** 021061
[47] Harris J, Yan B and Sinitsyn N A 2022 *Phys. Rev. Lett.* **129** 050602